A conditional sampling-based method for noise and resolution corrections for scalar dissipation rate measurements

Jian Cai and Chenning Tong[a)]
Department of Mechanical Engineering, Clemson University, Clemson, South Carolina 29634-0921, USA

A conditional sampling-based method for correcting noise and resolution effects for scalar dissipation rate measurements is developed. Noise and resolution effects on the measured dissipation rate have opposite trends, making their separation and accurate corrections difficult. A major task in dissipation rate correction, therefore, is to isolate each effect. The conditional-sampling method presented in this work uses instantaneous local scalar mean and variance as conditioning variables, and is based in part on Kolmogorov's refined similarity hypotheses. It ensures selection of instantaneous fully resolved local scalar fields, which are analyzed to determine the measurement noise. Noise correction is applied to potentially under-resolved local scalar fields, also selected using the conditional-sampling procedure, effectively separating the effects of noise from those of resolution. The error function is used as a model for the potentially under-resolved local scalar fields to evaluate their dissipation length scales and to make corrections for the dissipation rate. The present method uses local instead of spectral analyses; therefore, can be applied to the mean scalar dissipation rate conditional on the scalar values. An application of the method to temperature dissipation rate in a slightly heated turbulent jet shows excellent results, validating the method. The method can also be applied to other challenge situations, such as turbulent flames. © *2009 American Institute of Physics.*
[DOI: 10.1063/1.3147930]

I. INTRODUCTION

The scalar dissipation rate is an important variable characterizing turbulent mixing. It is the rate at which the variance of scalar fluctuations is reduced by molecular mixing. It is also a key variable in studying and modeling turbulent nonpremixed/partially premixed flames.[1,2] Much effort, therefore, has been devoted to measurements of the scalar dissipation rate. Because the scalar dissipation rate in a turbulent flow comes primarily from the smallest scalar length scales, its measurements require high spatial resolution. At the same time, the scalar fluctuations at these scales are generally much smaller than the energy-containing fluctuations, requiring low measurement noise to achieve an adequate signal-to-noise ratio for dissipation rate measurements. In practice, however, neither requirement is guaranteed. Often, the resolution of the measurement system is comparable to the smallest length scales and the noise contribution to the dissipation rate is significant, potentially resulting in nonnegligible errors in the measured dissipation rate.

Resolution and noise have different effects on dissipation rate measurements. The measured scalar dissipation rate decreases with measurement resolution. Measurement noise, however, is usually additive to the measured scalar; therefore, the noise contribution to the measured mean dissipation is always positive. The contribution generally increases with resolution (or smaller sample spacing) because the distance over which the derivatives are taken is reduced while the noise differences are generally independent of (or even in-

crease with) the resolution. Because the noise and resolution effects are generally present at the same time, these opposite trends make corrections difficult; therefore, a major task in noise and resolution corrections is to separate their effects.

Previous studies generally focused on one of the issues or considered the combined effects. The effects of the probe resolution on the dissipative scale turbulent velocity and scalar fluctuations were first studied by Wyngaard.[3–5] Using the spectral models of Corrsin[6] and Pao[7] he analyzed the attenuation of the dissipative scale velocity, vorticity, and scalar spectra due to the finite probe size. He found that a temperature resistance wire (cold wire) must have a length comparable to or smaller than the scalar dissipation length scale to resolve 98% of the mean scalar dissipation rate. Brown *et al.*,[8] Antonia and Mi,[9] Mi and Nathan[10] examined the effects of the probe separation when using two cold wires to measure the scalar dissipation rate. Tong and Warhaft[11] found that a probe separation of approximately one scalar dissipation length scale is needed to measure accurately the scalar derivative kurtosis, which is strongly influenced by large derivative fluctuations. For smaller separations the noise contribution becomes significant. These studies provided the understanding of the effects of noise and resolution, but the effects are not separated. The studies also highlighted the need for separating the two effects in order to make accurate corrections for noise and resolution effects.

To evaluate the resolution effects the scalar dissipation length scale is needed. One way to evaluate the resolution and the dissipation length scales is to measure the dissipation rate with a range of resolutions (or sample spacings) to de-

---
a)Electronic mail: ctong@ces.clemson.edu.

termine whether the measured mean dissipation rate is approaching an asymptotic value when the resolution is increased.[9,10] However, in such measurements noise is also present and its contribution increases with resolution. As a result, for high-resolution measurements the noise contributions become significant, making it difficult to evaluate the length scales.

Using spectral analysis, Wang et al.[12] considered the overall impact of a measurement system. They considered the effects of optical blurring, pixel size, numerical schemes, and noise. Wang and Barlow[13] used the method to evaluate the dissipation length scales in turbulent nonpremixed flames. In such spectral approaches for evaluating resolution and noise, if the spatial resolution and the signal-to-noise ratio are sufficiently high, the noise spectrum can often be determined because it is generally constant with respect to the wavenumber (i.e., white noise), and dominates the measured spectrum at wavenumbers higher than the signal cutoff wavenumber. However, when the scalar is not fully resolved or the signal-to-noise ratio is low, there are significant contributions from both the signal and noise. Consequently, it is generally not possible to separate the noise spectrum. Instead, a model spectrum including the noise contribution is needed to fit the measured spectrum by varying the length scale and the relative noise contribution to the model spectrum. These parameters then are regarded as the length scale and the noise contribution.

A limitation of spectral approaches is that while it can provide an overall assessment of the noise level and the measurement resolution for the mean dissipation rate, it is not suitable for the conditional scalar dissipation rate, $\langle \chi | \phi \rangle$, for two reasons, where χ and ϕ are the scalar dissipation rate and the scalar value respectively. First, the measurement noise in general depends on the scalar value. The noise spectrum provides no information on the dependence of the conditional noise variance on the scalar value. Second, the resolution requirement for the conditional dissipation rate is likely to vary with the scalar value, and spectral analysis, in general, cannot provide the information regarding this requirement. Consequently, it cannot be used to make corrections for the conditional dissipation rate. The conditional dissipation rate is a key mixing term evolving the scalar probability density function (PDF). Its value near the stoichiometric mixture fraction largely determines the reaction rate in nonpremixed flames.[1,2] It is also a key variable in several models for nonpremixed and partially premixed turbulent combustion. It is, therefore, essential to develop a correction method applicable to the conditional dissipation rate.

Another limitation of the spectral method is that it is a global analysis method. In turbulent passive scalar fields as well as in nonpremixed and partially premixed turbulent flames, the so-called ramp-cliff scalar structure[11,14–17] is usually present. The cliff is a highly local structure generating large local dissipation rate but does not necessarily contribute significantly to the spectrum (the authors are not aware of any spectral model that includes this contribution), making spectral analysis insensitive to the ramp-cliff structure. In addition, the spectrum calculated depends on the ratio of the length of the signal record (e.g., the image size in laser di-

agnostic techniques) to the thickness of the cliff. Furthermore, spectral analysis cannot be used to isolate these structures to determine their contributions to the conditional dissipation rate and to correct for the measured conditional dissipation rate; therefore, spectral analyses are generally not suitable for characterizing the ramp-cliff structure.

Recently Wang et al.[18] and Kaiser and Frank[19] used redundant signals to remove noise effects in temperature dissipation measurements in turbulent flames. The former study performed two-point Rayleigh scattering measurements. The noise variance is obtained by a second set of measurements with the two points overlapping each other. The latter study obtained the spectra of the temperature by cross correlating the signal with that from the adjacent pixels in a two-dimensional image using the assumption that the two signals are identical except the noise contributions. Wang et al.[20] used measurements in laminar flames to infer the noise variance.

In the present work we develop a local analysis approach, which uses conditional sampling to evaluate the noise contributions (see Sec. II and Refs. 21, 14, and 16 for the conditional-sampling procedure). This method does not require redundant signals and the assumption (or approximation) that the redundant signals are identical to the original signals. It does not rely on spectral analysis, allowing conditioning of the dissipation rate on the scalar value at the same location. The most important aspect of the method is the conditional-sampling procedure, which is based on Kolmogorov's refined similarity hypotheses[22] (see Sec. III for details). The procedure is used to select fully resolved (verified a posteriori) local scalar fields, effectively separating the noise effects from the resolution effects. The fully resolved local scalar fields then are used to determine the measurement noise. Because the conditional-sampling procedure makes use of the properties of turbulent scalar fields, it essentially can guarantee selection of fully resolved local scalar, even when the whole scalar field is not fully resolved. The experimentally determined noise is applied to potentially under-resolved conditional local scalar fields for noise correction. The noise-corrected dissipation rate then is used to evaluate the scalar dissipation length scales (relative measurement resolution), and to make corrections to the scalar dissipation for under-resolution.

In this method we make use of the different spectral response (or resolution) of finite difference schemes (or numerical stencils) of different order in determining the measurement noise and evaluating the measurement resolution. Unlike some of the previous methods, this method does not rely on varying the measurement resolution (or the sample spacing) to evaluate dissipation length scale and only one resolution is needed.

The present local analysis method has several advantages over previous methods: (1) The use of conditional sampling allows separation of noise from the resolution effects to evaluate the noise contribution and the dissipation length scales without redundant measurements or redundant signals. (2) It can be used to make corrections to the conditional dissipation rate. (3) It can capture the ramp-cliff structure and analyze its effects on the conditional dissipation rate,

which is not well represented in spectral correction methods. In the following we first describe conditional-sampling procedure, followed by discussions of the finite difference schemes and its role in determining measurement noise and evaluating the dissipation length scales (relative resolution). An application of the method to measurements of the temperature dissipation in a slightly heated turbulent jet is discussed in Sec. III. The conclusions are given in Sec. IV.

II. DESCRIPTION OF THE METHOD

A. Conditional-sampling method

We use the conditional-sampling technique that we developed to study the subgrid-scale (SGS) scalar mixing.[21,14,15,23,16,17] It uses two conditioning variables: the filtered (locally averaged) scalar,

$$\langle\phi\rangle_L = \int \phi(\mathbf{x'})G(\mathbf{x}-\mathbf{x'})d\mathbf{x'}, \tag{1}$$

and the SGS scalar variance (or local scalar variance)

$$\langle\phi''^2\rangle_L = \int \{\phi(\mathbf{x'})-\langle\phi\rangle_L(\mathbf{x})\}^2 G(\mathbf{x}-\mathbf{x'})d\mathbf{x'}, \tag{2}$$

where $\langle\cdot\rangle_L$ represent a locally averaged variable $\int(\cdot)G(\mathbf{x}-\mathbf{x'})d\mathbf{x'}$. Here G is a top-hat filter function.

The conditional-sampling method makes use of the properties of the turbulent scalar fields. Our previous studies[21,14,15,23,16] have shown that for small SGS variance (smaller than the mean SGS variance) the SGS scalar is well mixed. The statistics of such (conditional) fields are well described by the Kolmogorov–Obukhov–Corrsin theory. The locally averaged scalar dissipation rate and the scalar variance spectral transfer rate are lower than the mean scalar dissipation rate. In the spirit of the Kolmogorov's refined similarity hypotheses, the local conditional Péclet number is expected to be lower than that based on the unconditioned statistics; therefore, the scalar dissipation length scales for these fields are expected to be larger than the mean scalar dissipation length scale. By choosing sufficiently small SGS variance values, one can select local scalar fields with sufficiently large dissipation length scales so that they are well resolved by the measurement apparatus. This property of the local turbulent scalar fields is demonstrated by the experimental results [Figs. 2 and 11(a)].

For large SGS variance, the locally averaged conditional scalar dissipation rate and the spectral transfer rate are larger than their mean values. In addition, the SGS scalar is highly segregated and contains the so-called ramp-cliff structure.[11,14–16] The scalar dissipation rate is very large inside the cliffs. At the same time, the cliffs in the SGS scalar are likely to have smaller length scales. Using conditional sampling with SGS variance values much larger than the mean SGS variance, one can select local scalar fields that are potentially under-resolved to evaluate their dissipation length scales. These fields will be analyzed to determine the dissipation length scales and to correct for any under-resolution.

TABLE I. Coefficients for central finite difference schemes.

Order	a_1	a_2	a_3	a_4	a_5
2	1/2	0	0	0	0
4	8/12	−1/12	0	0	0
6	45/60	−9/60	1/60	0	0
8	672/840	−168/840	32/840	−3/840	0
10	2100/2520	−600/2520	150/2520	−25/2520	2/2520

Because this method makes use of the physics of the turbulent scalar fields, it does not require redundant measurements.

B. Finite difference schemes for calculating scalar derivative

To obtain the scalar dissipation rate, numerical (usually finite difference) schemes are needed to calculate the derivatives because experimental data generally are in the form of discrete samples. Different schemes involve different numbers of samples and different weights to the samples. Consequently, the calculated scalar dissipation rate and the noise contribution are scheme dependent. Here we discuss the finite different schemes used.

A generalized form of an explicit central finite difference scheme for the derivative is

$$h \cdot \widetilde{\frac{d\phi}{dx}} = a_1(\phi_1 - \phi_{-1}) + a_2(\phi_2 - \phi_{-2}) + a_3(\phi_3 - \phi_{-3})$$
$$+ a_4(\phi_4 - \phi_{-4}) + \cdots, \tag{3}$$

where h and $\widetilde{d\phi/dx}$ are the distance between adjacent samples and the estimated scalar derivative, respectively. Several selected schemes and their coefficients are listed in Table I.

All finite difference schemes have numerical errors. One way to quantify the errors is to examine the spectral responses of the schemes, which we discuss briefly. For more detailed discussions, see Ref. 24. Here we focus on explicit central finite difference schemes. Using Fourier transform, a suitable function $\phi(x)$ can be represented as a superposition of a series of harmonic basis functions, $e^{i\kappa x}$, where κ is the wavenumber. The maximum wavenumber that can be represented by a set of discrete samples is $\kappa_{max}=\pi/h$, the Nyquist wavenumber, and higher wavenumbers will be aliased to those below π/h, where h is the distance between adjacent samples. It is, therefore, useful to analyze finite difference schemes in the wavenumber domain.

We examine the behavior of the schemes using their responses to a harmonic function $\phi=\phi_m e^{i\kappa x}$ whose derivative is $d\phi/dx=i\kappa\phi_m e^{i\kappa x}$. The response of a finite difference scheme can be represented as a function of the nondimensional wavenumber $h\kappa$ $(0\le h\kappa\le\pi)$. From Eq. (3) the estimated derivative is[24]

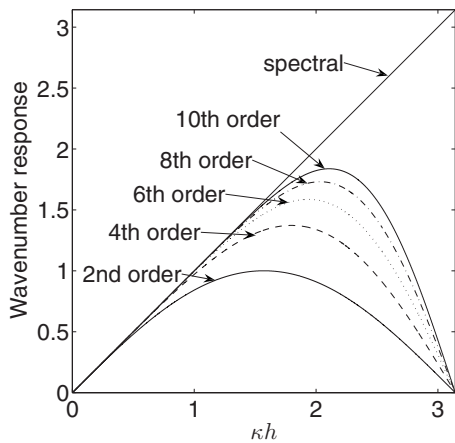FIG. 1. Spectral response as a function of wavenumber for selected finite difference schemes.

$$\widetilde{\frac{d\phi}{dx}}h = \sum_{n=-N}^{N} a_n \phi(x+nh)$$

$$= \sum_{n=1}^{N} a_n \phi_m (e^{i\kappa(x+nh)} - e^{i\kappa(x-nh)})$$

$$= 2i \sum_{n=1}^{N} a_n \phi_m \sin(n\kappa h) e^{i\kappa x}$$

$$= i\mathcal{R}(\kappa h)\phi_m e^{i\kappa x}, \tag{4}$$

where

$$\mathcal{R}(\kappa h) = \sum_{n=1}^{N} 2a_n \sin(n\kappa h)$$

is the response at wavenumber κ. In Eq. (4) $a_n = a_{-n}$. In the limit of $N \to \infty$, $\mathcal{R}(\kappa h) \to \kappa h$, which is the response of the spectral differentiation scheme. Also note that the response of a central finite difference scheme is a real function of wavenumber.

The wavenumber responses of several one-dimensional finite difference schemes have been discussed by Lele.[24] Figure 1 shows the spectral responses of the schemes given in Table I. All numerical differentiation schemes except spectral methods attenuate the wavenumbers near π/h. Lower-order schemes generally attenuate more severely than higher-order ones. For example, the second-order scheme (Table I) results in a 36.3% reduction at one-half of the Nyquist wavenumber whereas the tenth-order scheme attenuates 1.375%.

The spectral responses of the different schemes can be used to evaluate the measurement resolution and the scalar dissipation length scales. When a scalar field is resolved by all the schemes, the scalar derivative and the scalar dissipation rate obtained by these schemes are identical. For an under-resolved scalar field, higher-order schemes result in higher dissipation rates. Convergence of the dissipation rate as the scheme order increases would indicate that the scalar field is fully resolved by schemes of certain order or higher but not by the lower-order ones, providing an estimate of the length scale of the dissipation-scale scalar fluctuations. Even if no convergence is observed, the different dissipation rate values can be compared to a model with a known length scale to infer the scalar dissipation length scales.

To illustrate the effects of the responses of different schemes, we examine the finite difference estimation of the dissipation rate of an error-function scalar profile with a width of w,

$$\phi(x) = \mathrm{erf}\left(\frac{x}{w}\right) = \frac{2}{\sqrt{\pi}} \int_0^{x/w} e^{-x'^2} dx'. \tag{5}$$

Here w is proportional to the width of the scalar derivative profile. The dissipation rate is calculated at $\phi = 0$ where it is at its maximum. A comparison among the selected schemes is shown in Fig. 9. For a given scheme, as the distance between adjacent samples (h) increases, the calculated dissipation rate decreases. For a fixed h, higher-order schemes have better resolutions. (A very high-order scheme will approach the spectral method.) When noise is present in the samples, however, higher-order schemes generally result in higher noise contributions because these schemes involve more samples. As a result, without noise correction lower-order schemes tend to underestimate the dissipation rate, while higher-order ones tend to overestimate it. It is, therefore, essential to correct the noise effects before evaluating the resolution effects.

C. Effects of noise on dissipation rate measurement

The following discussion is based on the assumption that the noises at different measurement locations (be it different samples from a single probe or pixels of an imaging device) are uncorrelated and are additive to the scalar values. The measured scalar ϕ is

$$\phi = \phi^* + n, \tag{6}$$

where ϕ^* and n are the true scalar value and the noise, respectively. To correct for the noise contribution to the measured dissipation rate the noise variance needs to be determined. In general the noise variance depends on ϕ (such as measurements in flames),

$$\langle n^2 | \hat{\phi} \rangle = \sigma_n^2(\hat{\phi}), \tag{7}$$

where $\hat{\phi}$ is the sample-space variable for ϕ. For convenience, we do not explicitly write the sample-space variable hereafter. For the temperature dissipation rate measurement considered here, the noise from the resistance wire temperature sensor (or cold wire) is independent of the temperature signal and has a constant variance.

Including noise in the finite difference scheme in Eq. (3), the measured derivative is

$$h\widetilde{\frac{d\phi}{dx}} = a_1(\phi_1 - \phi_{-1}) + a_2(\phi_2 - \phi_{-2}) + a_3(\phi_3 - \phi_{-3}) + a_4(\phi_4 - \phi_{-4}) + \cdots$$

$$= a_1(\phi_1^* - \phi_{-1}^*) + a_2(\phi_2^* - \phi_{-2}^*) + a_3(\phi_3^* - \phi_{-3}^*) + a_4(\phi_4^* - \phi_{-4}^*) + \cdots$$

$$+ a_1(n_1 - n_{-1}) + a_2(n_2 - n_{-2}) + a_3(n_3 - n_{-3}) + a_4(n_4 - n_{-4}) + \cdots$$

$$= h \cdot \widetilde{\frac{d\phi^*}{dx}} + a_1(n_1 - n_{-1}) + a_2(n_2 - n_{-2}) + a_3(n_3 - n_{-3}) + a_4(n_4 - n_{-4}) + \cdots, \tag{8}$$

where $\widetilde{d\phi^*/dx}$ is the estimated derivative without noise. Note that such an estimated derivative is dependent on the scheme used due to the different spectral responses of different schemes. The measured mean dissipation rate is

$$\langle \widetilde{\chi} \rangle = \left\langle 2D \left(\widetilde{\frac{d\phi}{dx}} \right)^2 \right\rangle$$

$$= \left\langle 2D \left(\widetilde{\frac{d\phi^*}{dx}} \right)^2 \right\rangle + \left\langle \frac{2D}{h^2} \sum_{i=-N}^{N} a_i^2 n_i^2 \right\rangle$$

$$= \left\langle 2D \left(\widetilde{\frac{d\phi^*}{dx}} \right)^2 \right\rangle + \frac{2D}{h^2} \sum_{i=-N}^{N} a_i^2 \langle n^2 \rangle$$

$$= \left\langle 2D \left(\widetilde{\frac{d\phi^*}{dx}} \right)^2 \right\rangle + \frac{2D}{h^2} C_N \langle n^2 \rangle, \tag{9}$$

where $C_N = \Sigma_{i=-N}^{N} a_i^2$, D, and $\langle 2D(\widetilde{d\phi^*/dx})^2 \rangle$ are a scheme dependent factor, the molecular diffusivity, and the estimated dissipation rate without noise, respectively.

When all the schemes can resolve the turbulent scalar field, the measured mean dissipation rate $\langle 2D(\widetilde{d\phi^*/dx})^2 \rangle$ does not depend on the scheme. The measured mean dissipation rate versus C_N is a straight line, with a slope of $(2D/h^2)\langle n^2 \rangle$ and an intercept equal to the noise-corrected dissipation rate. This linear relationship can be used to determine the noise variance $\langle n^2 \rangle$.

When the resolution is reduced, the measured dissipation rate by the second-order scheme will fall below the straight line first because it is the least capable of resolving the dissipation rate. As the resolution is further reduced the fourth- and higher-order schemes will deviate from the linear relationship. On the other hand, as long as the eighth- and tenth-order schemes follow this straight line the dissipation is still fully resolved. The $\langle \chi \rangle - C_N$ plot, therefore, can be used to determine whether the scalar dissipation is fully resolved. In the following we employ the conditional-sampling method to select fully resolved local scalar fields and determine the noise variance according to Eq. (9). The noise variance is used to correct the dissipation rate for potentially under-resolved local scalar fields. The noise-corrected dissipation rates from the different schemes then are analyzed to evaluate the scalar dissipation length scales and to correct for resolution effects.

III. APPLICATION TO A SLIGHTLY HEATED TURBULENT JET

In this section the noise and resolution correction method discussed above is applied to the scalar dissipation rate of passive temperature fluctuations in a slightly heated turbulent jet.[21,14–16] The experimental data used in the present study were obtained in a heated turbulent jet. The jet facility was housed in a large, air conditioned room. The jet assembly was mounted vertically. A collection hood at a downstream distance of 260 nozzle diameters (3.9 m) minimizes the effects of the ceiling on the jet. Jet air supply was heated with a pipe heater before entering the plenum chamber, producing an excess temperature (above the ambient) of 20 °C at the nozzle exit.

Measurements were made for a jet exit velocity U_j of 40 m/s, which gives a jet Reynolds number Re_j of 40 000. The nozzle diameter D_j was 15 mm. Data were collected at a downstream distance of $x/D_j=80$ on the jet centerline. The effects of the initial jet-to-air density ratio (≈ 0.93) on the properties of the jet, such as the spreading rate and the rms fluctuations of velocity and temperature, were small.[25] Thus, in our measurements the temperature fluctuations were dynamically passive.

One-dimensional streamwise filtering was employed to compute the filtered scalar and the SGS scalar variance. The filtering was performed by invoking Taylor's hypothesis. Filter widths ranging from 5 to 40 mm were used, corresponding to $\Delta/\eta=31$ to 250. Here η (=0.16 mm) is the Kolmogorov scale. The scalar dissipation (or Obukhov–Corrsin) scale, η_ϕ, is 0.22 mm. The filter widths were chosen to be much larger than the dissipation scales.

Temperature fluctuations were measured with a platinum resistance wire of 0.6 mm in length and 0.625 μm in diameter, which has a frequency response up to 5 kHz. Details of the devices are given in Ref. 15. The temperature signals were low-pass filtered at 5 kHz and amplified by Krohn–Hite 3364 filter/amplifiers. The signals were digitized at 10 000 samples/second by a 12 bit National Instrument analog to digital converter (PCI-6071E). This sampling rate corresponds to a sample interval of 0.307 mm. The streamwise component of the scalar dissipation rate is measured using Taylor's hypothesis. In the following analyses we use data collected on the jet centerline where the mean velocity is 3.07 m/s. Only the fluctuating temperature is used, which is normalized by its rms values.
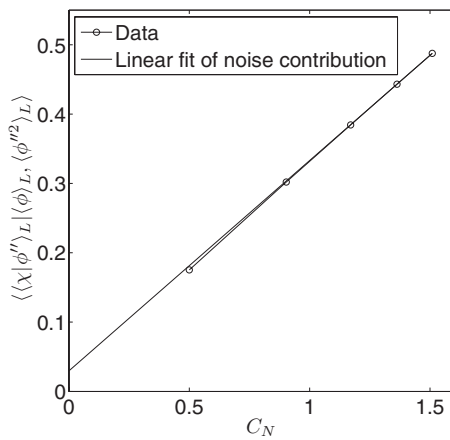
FIG. 2. Measured conditionally filtered dissipation rate $(1/s)$, $\langle\langle\chi|\phi''\rangle_L|\langle\phi\rangle_L,\langle\phi''^2\rangle_L\rangle$, vs C_N for $\langle\phi''^2\rangle_L=9.67\times10^{-4}$. Circles with increasing C_N values represent the second- to tenth-order schemes. The filter size is 20 mm and the scalar value ϕ'' is 0.0. The straight line is the best fit of the data points.

A. Conditional local scalar field

We first use small SGS variance values to select well-resolved local scalar fields, from which the conditionally filtered dissipation rates are calculated using the central difference schemes. As the scheme order increases, the conditionally filtered dissipation rate increases. We plot the conditional dissipation rate at $\phi''=0.0$ for a filter size of 20 mm ($\Delta/\eta=125$). Figure 2 shows that for $\langle\phi\rangle_L=0.0$ and $\langle\phi''^2\rangle_L=9.67\times10^{-4}$, $\langle\langle\chi|\phi''\rangle_L|\langle\phi\rangle_L,\langle\phi''^2\rangle_L\rangle$ as a function of C_N follows a straight line, indicating that for small SGS variance the local scalar fields are well resolved by all the schemes. The noise variance determined from this figure is 6.96×10^{-4}. Note that the intercept of the straight line (~0.02 s^{-1}) is much lower than the dissipation rate calculated using the second-order scheme (~0.17), indicating that even when using second-order scheme the noise contribution is greater than the true dissipation rate.

As the SGS variance value increases to $\langle\phi''^2\rangle_L=6.26\times10^{-3}$ (Fig. 3), the conditionally filtered dissipation rates obtained using the fourth- and higher-order schemes form a
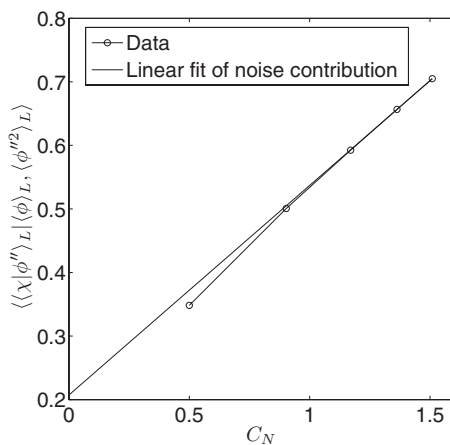

FIG. 3. Measured conditionally filtered dissipation rates vs C_N for $\langle\phi''^2\rangle_L=6.26\times10^{-3}$. Symbols same as in Fig. 2.
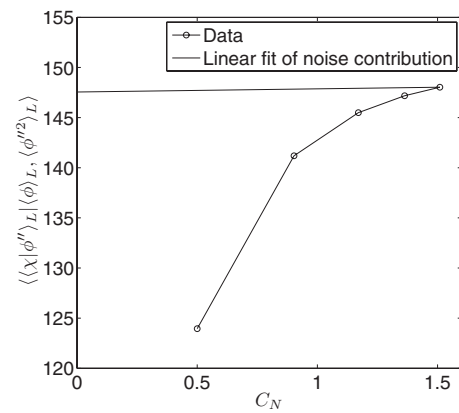

FIG. 4. Measured conditionally filtered dissipation rates vs C_N for $\langle\phi''^2\rangle_L=4.34$. Symbols same as in Fig. 2.

straight line while the dissipation rate using the second-order scheme is below this line, indicating that the higher-order schemes are capable of resolving the smallest scalar length scales in this case but second-order scheme is not. The slope of the line is very close to that in Fig. 2, indicating that the noise variance is determined accurately. In this case the noise-corrected conditionally filtered dissipation (the intercept) is of the same order of magnitude as (or smaller than) the noise contributions for the second- and fourth-order schemes, indicating that the conditional sampling and the use of the varying spectral response of the finite difference schemes of different orders allow accurate determination of the noise variance even when the noise contribution is greater than the dissipation rate.

For large SGS variance, $\langle\phi''^2\rangle_L=4.34$ (Fig. 4), the conditionally filtered dissipation rates using the eighth- and lower-order schemes are below the straight line going through the data point for the tenth-order scheme and having the same slope as that in Fig. 2, indicating that the eighth- and lower-order schemes are not capable of resolving all the scalar length scales. Note that the dissipation rate values obtained using the second- and fourth-order schemes are well below the intercept of straight line (~150 s^{-1}), indicating that even without correcting for noise these schemes are underestimating the dissipation rate. There is, however, no evidence to show that whether the tenth-order scheme is capable of fully resolving the scalar scales. A model for the scalar dissipation rate profile, therefore, is needed to evaluate the resolution.

B. Noise correction and resolution evaluation

The conditionally filtered dissipation rate for a range of scalar fluctuations obtained using the schemes for three SGS scalar variances, $\langle\phi''^2\rangle_L=9.67\times10^{-4}$, 6.26×10^{-3}, and 4.34, are given in Figs. 5(a), 6(a), and 7(a) respectively. All the figures show that the calculated dissipation rates increase as the order of schemes increases. The increases come from both noise and better resolution of higher-order schemes. In Figs. 5(b), 6(b), and 7(b) we show the results after subtracting the noise contributions determined in the previous subsection.
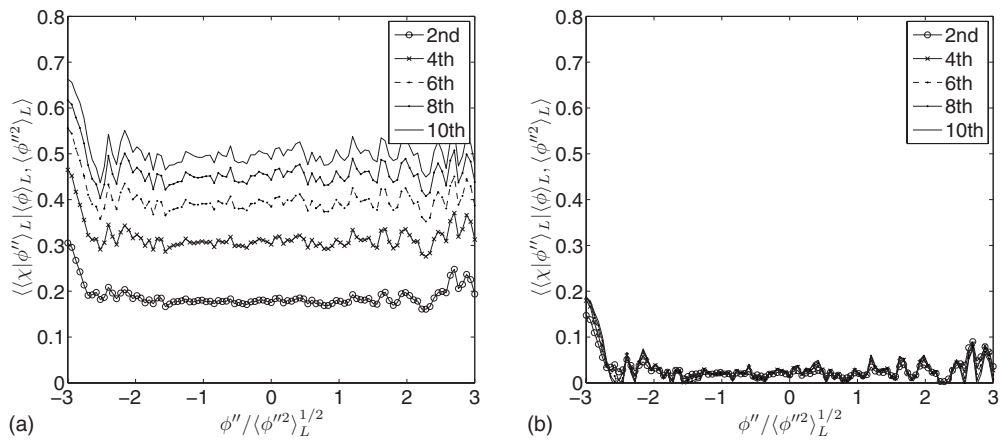
FIG. 5. Conditionally filtered dissipation rates before and after noise correction for $\langle\phi''^2\rangle_L = 9.67 \times 10^{-4}$.
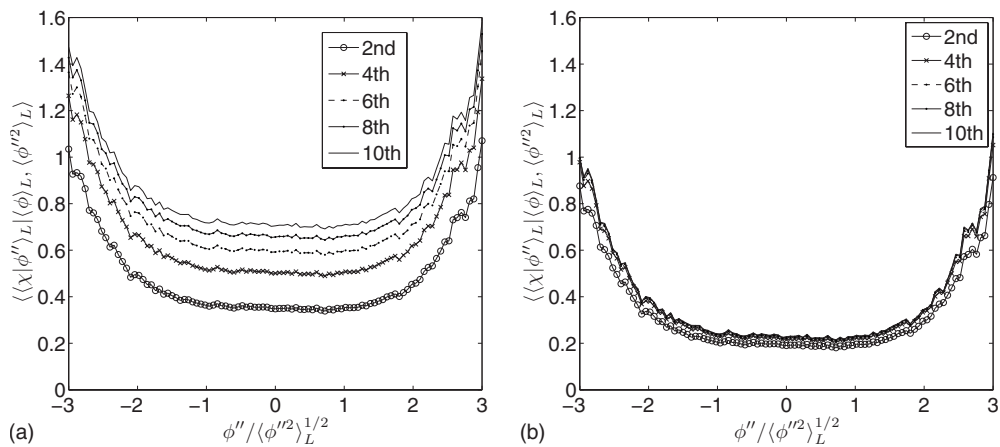

FIG. 6. Conditionally filtered dissipation rates before and after noise correction for $\langle\phi''^2\rangle_L = 6.26 \times 10^{-3}$.
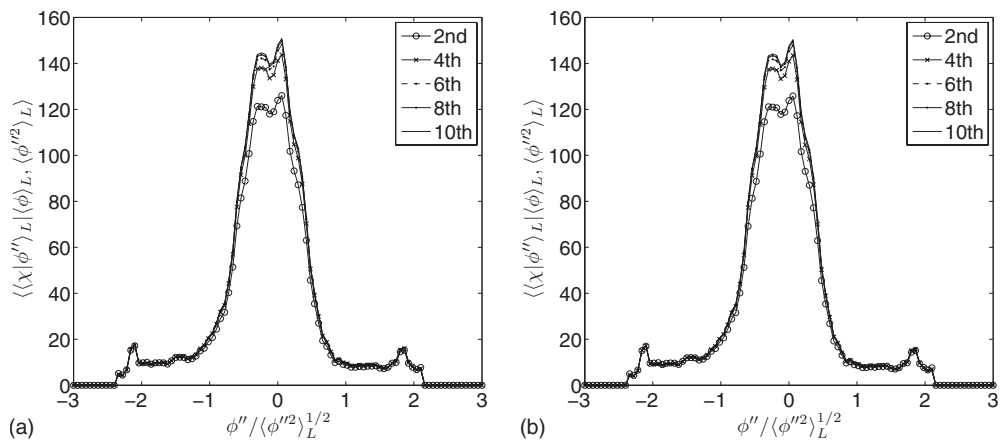

FIG. 7. Conditionally filtered dissipation rates before and after noise correction for $\langle\phi''^2\rangle_L = 4.34$.
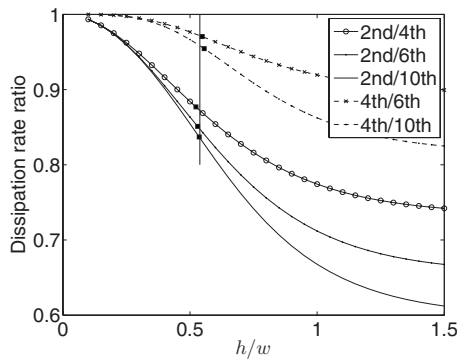
FIG. 8. Estimation of the scalar dissipation length scale by comparing the ratio of dissipation rates obtained using different schemes from the data and the model. Curves are ratios of dissipation rates using different schemes. Solid squares are the ratios calculated from the data.

For small SGS scalar variance (Fig. 5), the noise-corrected dissipation rate values calculated using second- to tenth-order schemes largely overlap, indicating that all the schemes are capable of resolving the scalar dissipation length scale and the noise correction is accurate. Increasing the SGS scalar variance to $\langle \phi''^2 \rangle_L = 6.26 \times 10^{-3}$ (Fig. 6), the conditionally filtered dissipation rates using fourth- or higher-order schemes overlap, consistent with Fig. 3, indicating that these schemes are sufficient to resolve all the scalar length scales and noise contributions have been removed.

For large SGS scalar variance (Fig. 7), the conditionally filtered dissipation rates for different schemes still show differences near $\phi''=0$ after the noise correction, indicating that the resolution requirement depends on the scalar value. The increase of the calculated dissipation rate from the second order to fourth order is large, indicating that the second-order scheme is far from having sufficient resolution. The differences between eighth- and tenth-order schemes are much smaller, indicating that the dissipation rates calculated using these schemes are close to the true dissipation rate.

After correcting for the noise, the measured dissipation rate is only affected by the measurement resolution, which is expected to be worst when the SGS scalar variance is large due to the steep cliffs present in the SGS scalar. Because the length scales of these cliffs are not known *a priori*, we need to use experimental data to infer them. In the present
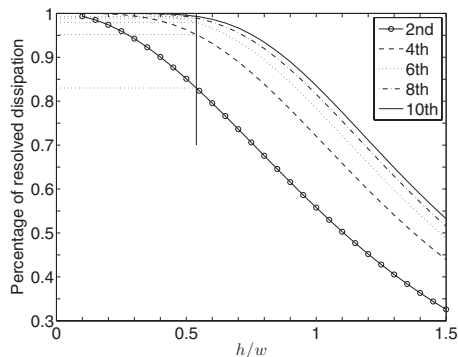

FIG. 9. Estimation of the percentage of the resolved dissipation rates of the error-function scalar profile using different finite difference schemes.
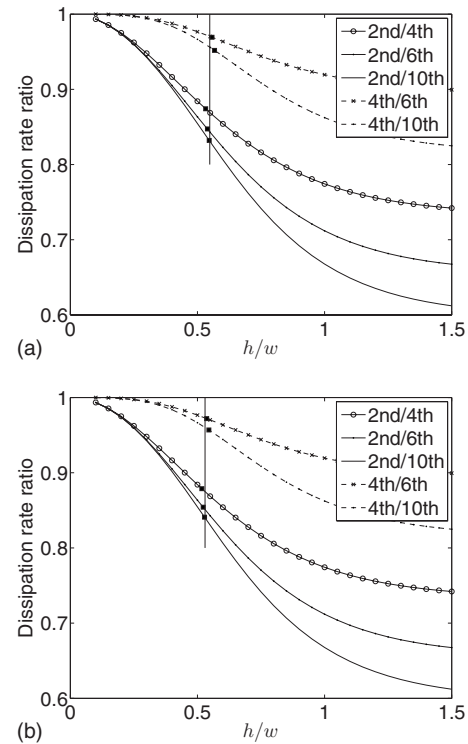

FIG. 10. Estimation of resolved dissipation length scale using the error-function model. (a) 5 mm filter size; (b) 40 mm filter size.

study, the Obukhov–Corrsin scale is estimated from the Kolmogorov scale. In a more complex flow (e.g., a turbulent flame) it is generally not possible to estimate accurately the local scalar dissipation length scale. In any case, the scales of the cliffs are not known. Comparing the measured scalar spectrum to a model spectrum can provide an estimate of the average length scale, but not those of the cliffs dominating the scalar dissipation rate for large SGS variance.

To estimate the length scales of the cliffs we use the error function [Eq. (5)] as a model for the ramp-cliff structure, and calculate its dissipation rate using different schemes with a range of sample intervals (spatial resolutions). The error-function profile is the canonical solution of the diffusion equation with an advective-diffusive balance. Tong and Warhaft (1994) found experimentally that there is a distribution of the cliff thickness ranging from the Kolmogorov scale to the Taylor microscale, with the average thickness scaling with the Taylor microscale, suggesting that they are a result of the balance between the large-scale strain rate and the molecular diffusivity. Buch and Dahm[26,27] showed experimentally that in general the dissipation layers have error-function profiles. The results in the present study (see below) are also consistent with the error-function profile, providing further evidence supporting the use of the error function as a profile for the ramp-cliff structure.

In order to infer the scalar dissipation scale we use the ratios of the dissipation rates calculated using schemes of different orders. By equating the ratios from the measurements and from the model, a scalar dissipation length scale can be inferred. The results are shown in Fig. 8. The horizontal axis is the ratio of sample interval to the scalar profile
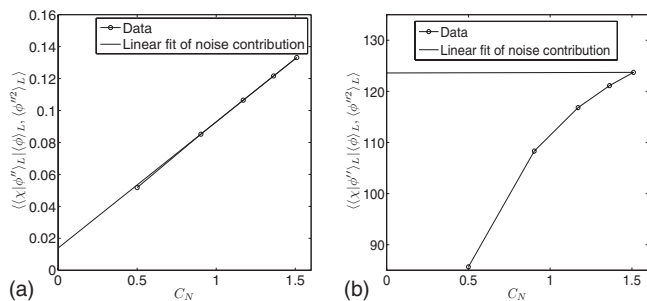
FIG. 11. Measured conditionally filtered dissipation rate, $\langle\langle\chi|\phi''\rangle_L|\langle\phi\rangle_L,\langle\phi''^2\rangle_L\rangle$, vs C_N for the double-spacing data (0.614 mm spacing). (a) $\langle\phi''^2\rangle_L=9.67\times10^{-4}$; (b) $\langle\phi''^2\rangle_L=4.34$. Circles with increasing C_N values represent the second- to tenth-order schemes. The filter size is 20 mm and the scalar value ϕ is 0.0. The straight line in (a) is the best fit of the data points. The straight line in (b) has the same slope as in (a).

FIG. 13. The filtered density function of the SGS scalar (PDF of the conditional local scalar fields) for $\langle\phi\rangle_L=0$ and $\langle\phi''^2\rangle_L^{1/2}=4.34$. The peaks have Gaussian-like shapes.

width, h/w. Here the ratios for the conditional dissipation rate at $\phi''=0.0$ are shown because at this scalar value the dissipation is the highest, corresponding to the smallest scalar length scale. These measured ratios are compared to the error-function model predictions to infer the length scale. For example, the ratio of the second order to the tenth order is approximately 0.84, giving a h/w of 0.54. This h/w value corresponds to 0.324 times the full width at half maximum (FWHM) of the scalar dissipation rate profile, which is $0.307/0.324=0.948$ mm. The scales inferred from the other schemes also agree very well, indicating the overall success of the noise correction and resolution/length scale evaluation. The h/w value can be used to correct for under-resolution. Figure 9 shows the fraction of the dissipation resolved by the schemes for a range of h/w values. With a sample interval of $h/w=0.54$ the second- to the tenth-order schemes underestimates the conditionally filtered dissipation rate by 17%, 5%, 2%, 1.1%, and 0.7%, respectively. Thus, sample interval of approximately $0.5w$ combined with a sixth- and higher-order finite difference scheme is able to resolve the dissipation rate with sufficient accuracy. Note that the peak conditionally filtered dissipation rate for large SGS variance comes from very large dissipation rate fluctuations and is much larger than the mean dissipation rate (4.20 s^{-1}).

The choice of filter size in the conditional-sampling method is not critical. Generally, it should be large compared
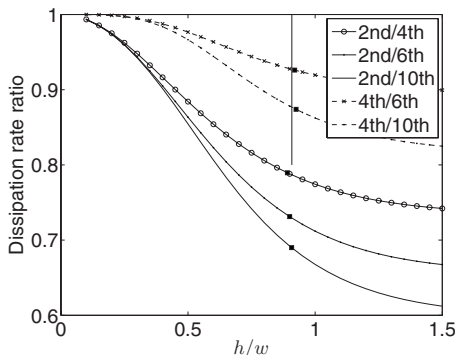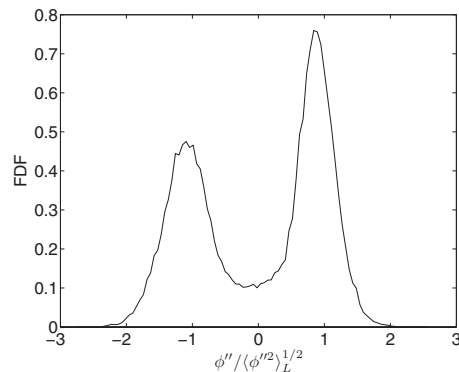
to the dissipation length scale so that the Kolmogorov–Obukhov–Corrsin theory applies to the conditional local scalar fields with small SGS variance. Here we use experimental data to show that the results are not sensitive to the filter size. Figure 10 shows the estimated scale (h/w) for the ramp-cliff structure for filter sizes, 5 and 40 mm, corresponding to $\Delta/\eta=31$ and 250, respectively. The scales inferred differ by less than 2%, sufficiently accurate for such dissipation rate measurements. We expect any filter size reasonably far away from the dissipation length scale (say $>10-15\eta$) to give accurate estimations.

In the case that the resolution is insufficient, the relative resolution inferred from Fig. 8 can be used to estimate the amount of under-resolution and make corrections using Fig. 9. To examine the effectiveness of the error-function model for severely underestimated scalar fields, we perform the same analysis for a sample interval of $h=0.614$ mm, twice that used above (0.307 mm). Figure 11(a) shows that the method still is capable of selecting the well-resolved local scalar fields (resolved by the sixth- to tenth-order schemes) to determine accurately the measurement noise. For large SGS variance the local scalar fields are severely under-resolved [Fig. 11(b)]. Using the procedure for obtaining the scale in Fig. 8, we estimate the h/w value for these scalar fields, which should be twice the value obtained for the

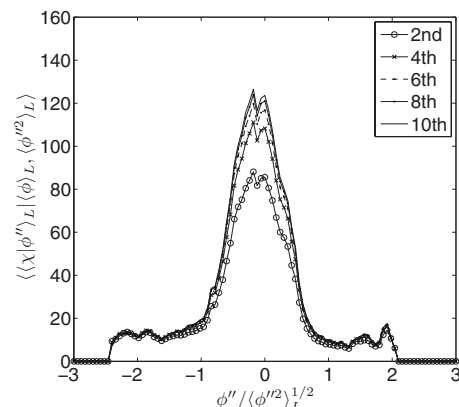FIG. 12. Estimation of the dissipation length scale for the double-spacing data. The SGS variance is 4.34.

FIG. 14. Conditionally filtered dissipation rates after noise correction for the double-spacing data with $\langle\phi''^2\rangle_L=4.34$.
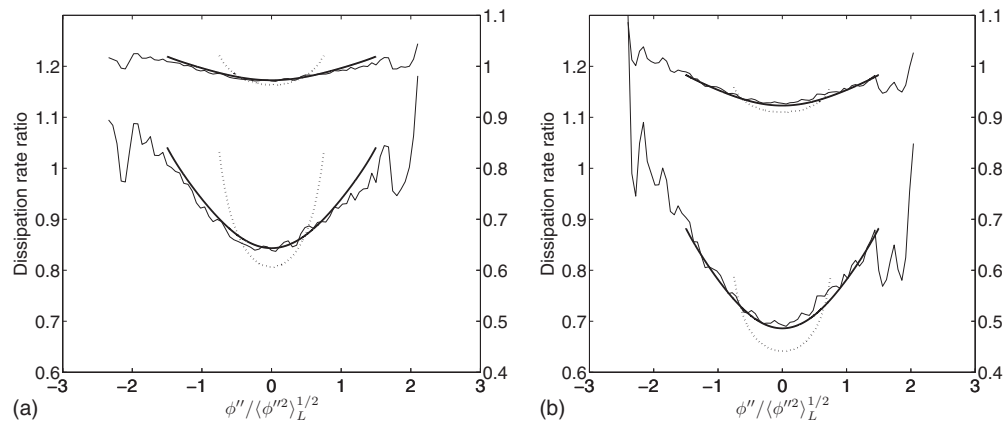
FIG. 15. The ratio of the conditionally filtered dissipation rate obtained using different finite difference schemes. Left ordinates: second- to tenth-order schemes. Right ordinates: fourth- to sixth-order schemes. The solid line, the thick solid line, and the dashed line represent experimental results, revised error-function model, and the original error-function model. (a) Single spacing; (b) double spacing. The SGS variance is 4.34.

single-spacing data $(2 \times 0.54 = 1.08)$ shown in Fig. 8. The estimated value, however, is 0.92, approximately 15% smaller than expected (Fig. 12).

To understand this discrepancy and to make corresponding corrections, we revisit the error-function model for the ramp-cliff structure. The model assumes that the error-function scalar profile ranges from -1 to 1. In reality, there are also "background" scalar fluctuations in addition to the ramp cliff in the local scalar fields. Thus, any dissipation value χ in the ramp-cliff structure no longer occurs at the ϕ value give by $\chi = \chi(\phi)$, but at values fluctuating around ϕ according to the distribution of the background scalar fluctuations. Figure 13 shows the conditional filtered density function (FDF), which is essentially the PDF for these conditional local scalar fields (see Refs. 21 and 14 for details). The two peaks have Gaussian-like shapes, suggesting that the FDF can be modeled as a convolution of a double-delta function and a Gaussian PDF. We revise the model to allow the scalar values in the error function to fluctuate in the scalar space, with the fluctuations having a Gaussian distribution as suggested by the peaks in Fig. 13. These background fluctuations also result in additional dissipation rate whose conditional mean is largely independent of the scalar value as shown in Fig. 14 for $\phi''/\langle\phi''^2\rangle_L^{1/2} < -1.5$ and $\phi''/\langle\phi''^2\rangle_L^{1/2} > 1.5$. Thus, a constant dissipation rate due to the background fluctuations, approximately 10 s^{-1}, is added to the modeled dissipation rate of the error-function profile.

The revised model is used to predict the ratios of the conditional dissipation rates obtained using schemes of different orders as a function of the SGS scalar value (Fig. 15). The predictions are compared with the experimental results. The h/w value is varied to find the best fit to the data. Detailed procedures for implementing the revised model are given in Appendix. The resulting value for the double-spacing data is $h/w = 1.15$, which is then used as the corrected h/w value for the ramp-cliff structure. The revised length scale is approximately 25% larger than the original estimation, indicating strong effects of the revised model taking into account the background fluctuations. We repeat this procedure for the single-spacing data and obtained an h/w value of 0.60, only 10% larger than the original prediction,

indicating that for reasonably well-resolved local fields the estimated length scale for the single-spacing data is affected to a much lesser degree by the background fluctuations. The revised value for the double-spacing data is within 4% of twice the h/w value for the revised single-spacing data, suggesting that the revised model provides a significant improvement over the original model.

The fluctuations of the ramp-cliff structure in the scalar space and the background scalar fluctuations also affect the model prediction of the fully resolved conditionally filtered dissipation rate (see Appendix). Our calculations show that the dissipation rate at $\phi'' = 0$ is reduced by 20% compared to the original error-function model [Eq. (5)]; therefore, the ratio of the revised model predictions using different schemes to the fully resolved dissipation rate are used and the results are shown in Fig. 16. Using the estimated h/w values the amount of under-resolution of the conditionally filtered dissipation rate can be estimated. For the single- and double-spacing data the tenth-order scheme underestimates the peak conditionally filtered dissipation rate by 1% and 19.3%, respectively. The ratio of these estimated dissipation rates is 0.817, consistent with the peak dissipation rate values in Figs. 7(b) and 14, which have a ratio of 0.84, further validating the revised error-function model. Note that the
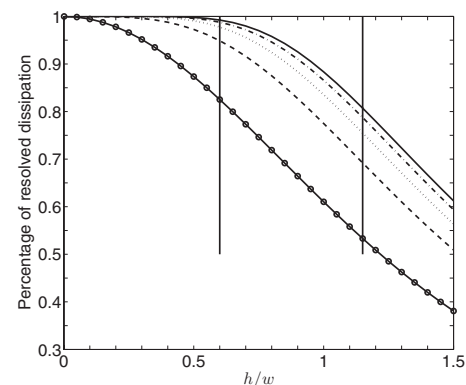

FIG. 16. The ratio of the resolved conditionally filtered dissipation rate from different schemes to the fully resolved conditionally filtered dissipation rate using the revised error-function model.

amounts of under-estimation for the original error-function model are 1% and 13%, respectively. The corrected values differ by only 6.7% for the double-spacing data, further demonstrating the robustness of the present method.

IV. CONCLUSIONS

A conditional sampling-based method for noise and resolution corrections for scalar dissipation rate measurements is developed and demonstrated using experimental data obtained in a turbulent jet. The method employs a conditional-sampling procedure to separate the noise from resolution effects, both strongly influencing the accuracy of dissipation rate measurements.

The conditional-sampling method makes use of the properties of local turbulent scalar fields based on Kolmogorov's refined hypotheses. These properties are demonstrated by the experimental results [Figs. 2 and 11(a)]. The filtered scalar value and the SGS scalar variance are used as conditioning variables. The procedure ensures the selection of well-resolved local scalar fields by using sufficiently small SGS variance values, allowing determination of the contribution from measurement noise to the measured scalar dissipation rate without redundant measurements. The experimentally determined noise variance is used to correct potentially under-resolved local scalar fields, effectively separating the effect of noise from that of resolution. The noise-corrected dissipation rate then is used to estimate the scalar dissipation length scale (the relative measurement resolution) and to make corrections for insufficient resolution.

Explicit finite difference schemes of different orders are used to calculate the scalar derivative. For the well-resolved local scalar fields, all the schemes should give the same dissipation rate, and any differences are due to the measurement noise. The spectral responses and the noise contributions of the schemes are exploited to determine the measurement noise. The results confirm that these fields are indeed well resolved. The noise variance then is determined from the data.

For potentially under-resolved local scalar fields selected using large SGS variance values, the data are used first to examine the extent of under-resolution. For local scalar fields that cannot be resolved by the eighth-order scheme, the error-function model is used to estimate the scalar dissipation length scale (FWHM of the scalar dissipation rate profiles). The model then is revised to allow fluctuations of the error-function scalar profile in the scalar space due to the background scalar fluctuations, and to include the background dissipation rate. The ratios of the measured dissipation rates obtained using different schemes are compared to the model calculations to infer the dissipation length scale. The results demonstrate the validity of the error function as a model for the ramp-cliff scalar profile when the SGS variance is large.

We find that a sample spacing of 0.307 mm (single spacing) combined with an eighth or higher-order scheme is capable of resolving more than 99% of the largest conditionally filtered dissipation rate at the measurement location. Note that when the SGS variance is large the dissipation rate (≈ 150 s^{-1}) is much larger than the mean dissipation rate

(4.20 s^{-1}); therefore, the mean dissipation rate is even better resolved. For a sample spacing of 0.614 mm (double spacing), only 80.7% of the largest conditionally filtered dissipation rate is resolved; however, the estimated length scale can be used to correct the dissipation rate to within 4%. The method can also be applied to even less resolved fields. Figure 12 suggests that the method has sufficient sensitivity at least up to $h/w=1.5$ ($h=0.9$ FWHM). For more severely under-resolved fields we expect the estimation will be less accurate but the method is still expected to be capable of providing a vastly improved dissipation rate estimation over the uncorrected one.

The present method can provide the dissipation length scale, guide selection of a measurement system resolution using a preliminary run, and be used to make corrections for noise and under-resolution. The conditional dissipation rate (without filtering) can be evaluated first by plotting its values obtained using different schemes (such as in Fig. 2) without conditioning on the SGS variance. If the resolution is sufficient, the noise-corrected conditional dissipation rate is obtained. If the resolution is insufficient, it can be obtained by summing the conditionally filtered dissipation rate for all the bins weighed by the probability for each bin. The correction procedure for under-resolution is applicable for all SGS fields having bimodal FDFs, including some having intermediate values of the SGS variance. In practice, for a measurement system with a reasonable resolution, only the bins with the highest SGS variance values should need significant corrections for under-resolution. The lower bins most likely only need noise correction and can be combined as one large bin. In the case that bins with unimodal FDFs are also under-resolved, the measurement system is probably not suitable for the intended flow.

The present study shows that the local analysis method based on the conditional-sampling procedure is capable of correcting noise and resolution effects accurately for a sample spacing twice (or even larger) of the spacing required to fully resolve the scalar field. The choice of filter size is not critical. Generally, filter sizes ranging from 10 to 15 Kolmogorov scales to one-fourth of the integral length scale can be used. The parameters in the revised model are deduced from the experimental data; therefore, the procedure is very robust.

The method has several advantages over previous methods: (1) The use of conditional sampling allows separation of noise from the resolution effects to evaluate the noise contribution and dissipation length scales, and to make accurate corrections. The conditional sampling and the use of the varying spectral response of the finite difference schemes of different orders allow accurate determination of the noise variance, even when the noise contribution is greater than the dissipation rate. We emphasize that the conditional-sampling procedure for selecting local scalar fields is based on the physics of turbulence. The basis for selecting the fully resolved local scalar fields is Kolmogorov's refined similarity hypotheses. To our best knowledge, this is the first time that the concept of K62 is being used for such a purpose. The basis for selecting the local scalar fields containing the ramp-cliff structure is based on the authors' recent work on the

filtered density function and dissipation of subgrid-scalar fields. The conditional-sampling procedure, therefore, makes use of the physics of the turbulence to extract information for analyzing the measurement noise and resolution. This method is in contrast to previous techniques in that for noise correction no external input such as redundant measurements or spectral models beside the data is needed. (2) It is applicable to the conditional dissipation rate, which is essential for many applications. (3) It can capture the effects of the ramp-cliff structure on the conditional dissipation rate. The ramp-cliff structure is local in space and is not well represented in spectral correction methods.

The method can be extended to more complex situations such as turbulent flames where noise is dependent on species mass fractions and temperature, and dissipation length scale is not uniform (larger in the reaction zone). When laser diagnostic techniques are used in flames the noise often is shot-noise limited and the noise variance is dependent on the scalar. For example, in mixture fraction measurements the noise variance is often proportional to mixture fraction. For such data, the mean dissipation rate in Eq. (9) is replaced by the conditional mean of the measured dissipation rate. The conditional noise variance then can be obtained from the procedure described above. Note that because the noise depends on the scalar, spectral analysis is not capable of obtaining the conditional noise variance. An application of the present method to scalar dissipation rate measurements in turbulent partially premixed flames shows similar results and will be published in a separate paper.

ACKNOWLEDGMENTS

APPENDIX: REVISED ERROR-FUNCTION MODEL FOR RAMP-CLIFF STRUCTURE

The ramp-cliff model assumes an error-function scalar profile; therefore, the dissipation rate has a Gaussian profile in physical space,

$$\chi(x) = 2D\left(\frac{d\phi}{dx}\right)^2 = \frac{8D}{\pi w^2}e^{-2(x/w)^2}. \tag{A1}$$

After substituting the physical-space variable with the scalar value ($x = w\,\mathrm{erf}^{-1}(\phi)$), the dissipation-rate profile in scalar space is

$$\chi(\phi) = \frac{8D}{\pi w^2}\exp(-2(\mathrm{erf}^{-1}(\phi))^2), \quad \text{where} -1 < \phi < 1. \tag{A2}$$

This dissipation rate is defined only for $-1 < \phi < 1$. There are, however, background scalar fluctuations in addition to the ramp cliff, which result in fluctuations of the dissipation $\chi(\phi)$ in scalar space as well as background dissipation. These effects can be modeled by statistically shifting the error-function scalar profile in scalar space and a constant

background dissipation. To do this, we first extend $\chi(\phi)$ as follows:

$$\chi_e(\phi) = \begin{cases} \dfrac{8D}{\pi w^2}\exp(-2(\mathrm{erf}^{-1}(\phi))^2), & -1 < \phi < 1; \\ 0, & \text{otherwise}. \end{cases} \tag{A3}$$

The shifting in scalar space is accounted for by convolving $\chi_e(\phi)$ with a Gaussian kernel in scalar space,

$$G(\phi, \psi; \sigma) = \frac{1}{\sqrt{2\pi}\sigma}e^{-(\phi-\psi)^2/2\sigma^2}, \tag{A4}$$

which represents the distribution of the "background" fluctuations. The kernel width is determined by fitting Gaussian distributions to the two branches of the FDF but excluding the part near $\phi'' = 0$. In this study, the width σ is between 0.38 and 0.39, and a value of 0.385 is used for the calculation. The resulting dissipation rate model as a function of the scalar space variable is

$$\langle\chi|\phi\rangle_m = \int \chi_e(\psi)G(\phi,\psi;\sigma)d\psi + \chi_b$$

$$= \int_{-1}^{1} \frac{8D}{\pi w^2}e^{-2(\mathrm{erf}^{-1}(\psi))^2}\frac{1}{\sqrt{2\pi}\sigma}e^{-(\phi-\psi)^2/2\sigma^2}d\psi + \chi_b, \tag{A5}$$

where $\langle\chi|\phi\rangle_m$ and χ_b are the fully resolved conditional dissipation rate of the revised error-function model and the background dissipation rate, respectively. The background dissipation rate can be determined from the part of the noise-corrected dissipation that is independent of the scalar values. (See the following for the actual implementation.)

The dissipation rate of the revised error-function model calculated using a finite difference scheme is obtained by first writing down an analytical expression for the dissipation rate of an error-function profile calculated using the scheme,

$$\chi_N(x) = 2D\left(\frac{d\phi}{dx}\right)^2 = 2D\left(\frac{1}{h}\sum_{n=-N}^{N} a_n\phi(x+nh)\right)^2$$

$$= \frac{2D}{h^2}\left(\sum_{n=-N}^{N} a_n\mathrm{erf}\left(\frac{x+nh}{w}\right)\right)^2. \tag{A6}$$

Here $\chi_N(x)$ is a continuous function in physical space. After substituting the physical space variable with the scalar value $[x = w\,\mathrm{erf}^{-1}(\phi)]$, the resulting expression, which is a function of the scalar variable, is convolved with the Gaussian kernel:

$$\langle\chi|\phi\rangle_{m,N} = \int_{-1}^{1}\frac{2D}{h^2}\left(\sum_{n=-N}^{N} a_n\mathrm{erf}\left(\mathrm{erf}^{-1}(\psi)\right.\right.$$

$$\left.\left. + n\frac{h}{w}\right)\right)^2\frac{1}{\sqrt{2\pi}\sigma}e^{-(\phi-\psi)^2/2\sigma^2}d\psi + \chi_b, \tag{A7}$$

where $\langle\chi|\phi\rangle_{m,N}$ is the dissipation rate calculated with a $2N$th order scheme. The integration here is performed numerically for a range of ϕ values. In this case, the background dissipation rate is approximately 10 s^{-1} for $|\phi''/\langle\phi''^2\rangle_L^{1/2}| > 1.5$. In

the calculation, χ_b is determined by equating $\chi_b/\langle\chi|0\rangle_{m,N}$ to the measured ratio of the background to the peak dissipation at $\phi''=0$. The ratios of $\langle\chi|\phi\rangle_{m,N}$ obtained from different schemes then are compared with experimental results in Fig. 15.

[1] R. W. Bilger, "The structure of turbulent nonpremixed flames," Proc. Combust. Inst. **22**, 475 (1988).

[2] N. Peters, *Turbulent Combustion* (Cambridge University Press, Cambridge, 2000).

[3] J. C. Wyngaard, "Measurements of small-scale turbulence structure with hot wires," J. Sci. Instrum. **1**, 1105 (1968).

[4] J. C. Wyngaard, "Spatial resolution of the vorticity meter and other hot-wire arrays," J. Sci. Instrum. **2**, 983 (1969).

[5] J. C. Wyngaard, "Spatial resolution of a resistance wire temperature sensor," Phys. Fluids **14**, 2052 (1971).

[6] S. Corrsin, "Further generalization of Onsager's cascade model for turbulent spectra," Phys. Fluids **7**, 1156 (1964).

[7] Y.-H. Pao, "Structure of turbulent velocity and scalar fields in large wavenumbers," Phys. Fluids **8**, 1063 (1965).

[8] L. W. B. Brown, R. A. Antonia, and A. J. Chambers, "Effects of the separation between cold wires on the spatial derivatives of temperature in a turbulent flow," Boundary-Layer Meteorol. **27**, 129 (1983).

[9] R. A. Antonia and J. Mi, "Corrections for velocity and temperature derivatives in turbulent flows," Exp. Fluids **14**, 203 (1993).

[10] J. Mi and G. J. Nathan, "Corrections for velocity and temperature derivatives in turbulent flows," Exp. Fluids **34**, 687 (2003).

[11] C. Tong and Z. Warhaft, "On passive scalar derivative statistics in grid turbulence," Phys. Fluids **6**, 2165 (1994).

[12] G.-H. Wang, N. T. Clemens, R. S. Barlow, and P. L. Varghese, "A system model for assessing scalar dissipation measurement accuracy in turbulent flows," Meas. Sci. Technol. **18**, 1287 (2007).

[13] G.-H. Wang and R. S. Barlow, "Spatial resolution effects on the measurement of scalar variance and scalar gradient in turbulent nonpremixed jet flames," Exp. Fluids **44**, 633 (2008).

[14] D. Wang and C. Tong, "Conditionally filtered scalar dissipation, scalar diffusion, and velocity in a turbulent jet," Phys. Fluids **14**, 2170 (2002).

[15] A. G. Rajagopalan and C. Tong, "Experimental investigation of scalar-scalar-dissipation filtered joint density function and its transport equation," Phys. Fluids **15**, 227 (2003).

[16] D. Wang and C. Tong, "Experimental study of velocity-scalar filtered joint density function for LES of turbulent combustion," Proc. Combust. Inst. **30**, 567 (2005).

[17] D. Wang, C. Tong, R. S. Barlow, and A. N. Karpetis, "Experimental study of scalar filtered mass density function in turbulent partially premixed flames," Proc. Combust. Inst. **31**, 1533 (2007).

[18] G.-H. Wang, N. T. Clemens, and P. L. Varghese, "Two-point, high-repetition-rate Rayleigh thermometry in flames techniques to correct for apparent dissipation induced by noise," Appl. Opt. **44**, 6741 (2005).

[19] S. A. Kaiser and J. H. Frank, "Imaging of dissipative structures in the near field of a turbulent non-premixed jet flame," Proc. Combust. Inst. **31**, 1515 (2007).

[20] G.-H. Wang, R. S. Barlow, and N. T. Clemens, "Quantification of resolution and noise effects on thermal dissipation measurements in turbulent non-premixed jet flames," Proc. Combust. Inst. **31**, 1525 (2007).

[21] C. Tong, "Measurements of conserved scalar filtered density function in a turbulent jet," Phys. Fluids **13**, 2923 (2001).

[22] A. N. Kolmogorov, "A refinement of previous hypothesis concerning the local structure of turbulence in a viscous incompressible fluid at high Reynolds number," J. Fluid Mech. **13**, 82 (1962).

[23] D. Wang, C. Tong, and S. B. Pope, "Experimental study of velocity filtered joint density function and its transport equation," Phys. Fluids **16**, 3599 (2004).

[24] S. K. Lele, "Compact finite differences schemes with spectral like resolution," J. Comput. Phys. **103**, 16 (1992).

[25] R. W. Schefer and R. W. Dibble, "Mixture fraction field in a turbulent nonreacting propane jet," AIAA J. **39**, 64 (2001).

[26] K. A. Buch and W. J. A. Dahm, "Experimental study of the fine-scale structure of conserved scalar mixing in turbulent shear flows, Part 1. $Sc \gg 1$," J. Fluid Mech. **317**, 21 (1996).

[27] K. A. Buch and W. J. A. Dahm, "Experimental study of the fine-scale structure of conserved scalar mixing in turbulent shear flows, Part 2. $Sc \approx 1$," J. Fluid Mech. **364**, 1 (1998).